JOURNAL OF GUIDANCE, CONTROL, AND DYNAMICS
Vol. 32, No. 5, September–October 2009

Path Planning Algorithms for Skid-to-Turn Unmanned Aerial Vehicles

Nobuhiro Yokoyama* and Yoshimasa Ochi†
National Defense Academy, Yokosuka 239-8686, Japan

DOI: 10.2514/1.41822

This study describes two types of algorithms for skid-to-turn unmanned aerial vehicles to plan paths between two waypoints under constant wind conditions. The first type of algorithm is a rigorous optimization algorithm based on the Euler–Lagrange formulation with analytical integration of the path. The second type of algorithm is a fast algorithm describing the path by two circular arcs connected by a line segment or another circular arc in the air mass frame, which is similar to the Dubins path. The latter algorithm is developed for actual airborne application, whereas the former algorithm is developed to check the quasi-optimality of the path calculated by the latter algorithm. We present a convergence proof of the latter algorithm under certain assumptions and its quasi-optimality in comparison with the former algorithm. Furthermore, the computational efficiency and the convergence reliability of the latter algorithm are demonstrated through numerical examples.

Nomenclature

a_c	=	intermediate variable to calculate a_β and a_ψ, $\mathrm{N}^2 \cdot \mathrm{m} \cdot \mathrm{s}$
a_β	=	effectiveness of side-force control surface to sideslip angle
a_ϕ	=	effectiveness of roll angle to heading rate, 1/s
a_ψ	=	effectiveness of side-force control surface to yaw angle, 1/s
$a_\bullet$, $b_\bullet$	=	center of circular arc, m
c_f, c_v	=	coefficients of forces, N
c_p, c_r	=	coefficients of moments, $\mathrm{N} \cdot \mathrm{m} \cdot \mathrm{s}$
c_1, c_2, c_3, c_4	=	intermediate variables to calculate the switching time
D	=	drag, N
d	=	distance from terminal waypoint to interception point in the air mass frame, m
F_f, F_v	=	forces generated by the side-force control surface and fixed vertical fin, N
g	=	gravitational acceleration, $\mathrm{m/s^2}$
H	=	Hamiltonian
I_{xx}, I_{yy}, I_{zz}	=	moments of inertia, $\mathrm{kg} \cdot \mathrm{m}^2$
L	=	counterclockwise circular arc with $\delta_r = -\delta_{r\max}$
$l(\bullet)$	=	path length, m
l_f	=	difference of x coordinate between action point of F_f and center of gravity, m
l_v	=	difference of x coordinate between action point of F_v and center of gravity, m
$M(x)$	=	function that maps x to $x + 2n\pi$ by using an integer n such that $0 \leq x + 2n\pi \leq 2\pi$, rad
M_{zp}, M_{zr}	=	yawing moments generated by roll and yaw damping, $\mathrm{N} \cdot \mathrm{m}$
m	=	mass, kg
P_k	=	intermediate variable to calculate the path
p, q, r	=	angular velocity components in the body frame, rad/s
R	=	clockwise circular arc with $\delta_r = \delta_{r\max}$
S	=	line segment with $\delta_r = 0$
$T_p(d)$	=	time for the vehicle to arrive at the point of interception, s
$T_{vt}(d)$	=	time for the virtual target to arrive at the point of interception, s
t	=	time, s
u, v, w	=	airspeed components in the body frame, m/s
V	=	magnitude of the airspeed, m/s
w_x, w_y	=	wind components in the inertial frame, m/s
x, y	=	position of vehicle in the inertial frame, m
$\tilde{x}$, $\tilde{y}$	=	position of vehicle in the air mass frame, m
α	=	angle of attack, rad
β	=	sideslip angle, rad
$\hat{\beta}$	=	negative value of the maximum sideslip angle (i.e., $\hat{\beta} \triangleq -a_\beta \delta_{r\max}$), rad
γ	=	intermediate variables to calculate the path length
δ_r	=	deflection angle of the side-force control surface, rad
$\bar{\delta}_r$	=	δ_r corresponding to minimum Hamiltonian, rad
$\zeta_\bullet$, $\eta_\bullet$	=	intermediate variables to calculate the intersection point, m
λ_x, λ_y, λ_ψ	=	adjoints, s/m, s/m, s/rad
ρ	=	minimum turn radius of the vehicle [i.e., $\rho \triangleq V/(\lvert a_\psi \rvert \delta_{r\max})$], m
ψ, θ, ϕ	=	Euler angles, rad
$\chi_\bullet$	=	angle perpendicular to ψ, rad

Subscripts

$c1$, $c2$	=	intersection point
e	=	value at terminal time
f	=	specified terminal condition or circular arc approaching to virtual target
k	=	value at the beginning of the arc or segment
l	=	anticlockwise circular arc with $\delta_r = -\delta_{r\max}$
m	=	middle circular arc or line segment
max	=	maximum value
r	=	clockwise circular arc with $\delta_r = \delta_{r\max}$
ε, ε_1, ε_2, ε_3	=	small positive values, m
ε_4	=	small value, m
μ, ν	=	arc lengths at singular point, m
ξ	=	length of circular arc within the range of $[0, \pi\rho]$, m

Presented as Paper 6637 at the AIAA Guidance, Navigation, and Control Conference and Exhibit, Honolulu, HI, 18–21 August 2008; received 27 October 2008; revision received 11 April 2009; accepted for publication 11 April 2009.

*Research Associate, Department of Aerospace Engineering, Hashirimizu 1-10-20. Member AIAA.

†Professor, Department of Aerospace Engineering, Hashirimizu 1-10-20. Senior Member AIAA.

σ = length of circular arc within the range of $[\pi\rho, 2\pi\rho]$, m
0 = specified initial condition or circular arc starting from the initial waypoint

Introduction

A WIDE variety of small unmanned aerial vehicles (UAVs) have been developed over the past 10 years, and the range of application of such UAVs is expanding, mainly in the fields of surveillance and reconnaissance [1]. The present study focuses on small skid-to-turn UAVs, which turn in flight by deflecting control surfaces that generate side forces, thereby directly generating centripetal force without banking. By virtue of skid-to-turn procedures, a vehicle can maintain wings-level flight during a turn, affording the following advantages:

1) The reception of Global Positioning System signals and the reception/transmission of data link signals are more stable than in bank-to-turn vehicles, in which these signals are sometimes blocked by a banked wing.

2) It is possible to design simpler control laws of the camera angles for capturing a target in skid-to-turn vehicles, because the skid-to-turn control mechanism has less of an effect on the line of sight from the camera to the target in comparison with the bank-to-turn control mechanism. However, it should also be noted that techniques have been developed to incorporate the control laws of camera angles into the flight dynamics of bank-to-turn vehicles [2,3].

The use of skid-to-turn, rather than bank-to-turn, flight procedures necessarily alters the kinematics of a UAV and therefore influences the optimal path planning, an important function of UAVs in achieving autonomous operations. Optimal path planning is typically formulated as the process of finding the two-dimensional minimum-time path between two or more waypoints, taking the kinematics of the vehicle into account. The problem of the two-dimensional minimum-time path from an initial position and orientation to a final position and orientation in the no-wind case has been solved analytically by geometric arguments [4] and by optimal control theory [5,6]. The minimum-time path in the no-wind case is often referred to as the Dubins path and is described by a set of two circular arcs connected by either a line segment or an additional circular arc that is tangent to both of these arcs. The Dubins path has been modified, and its application has been extended to cases that include a vehicle that moves both forward and backward [6,7], constant wind [8] and wind vector fields [9], multiple waypoints [10], and obstacle avoidance [11]. If these considerations are applied to the path planning of bank-to-turn UAVs, the kinematics are given by the following:

$$\dot{x} = V\cos\psi + w_x \tag{1}$$

$$\dot{y} = V\sin\psi + w_y \tag{2}$$

$$\dot{\psi} = a_\phi \phi \tag{3}$$

$$|\phi| \le \phi_{\max} \tag{4}$$

where turn coordination is assumed and additional dynamics are neglected. However, Eqs. (1–4) are not valid for skid-to-turn UAVs. As will be shown in the next section, an effect of the deflection of the side-force control surface δ_r appears in the kinematics of skid-to-turn UAVs, and hence the direction of the inertial velocity vector may change instantaneously. Thus, some kinks may occur in the horizontal paths as opposed to the smoothness in the Dubins paths. To the best of the authors' knowledge, practical path planning algorithms that take into consideration the inherent kinematics of skid-to-turn UAVs have not been investigated, although the guidance and control laws for skid-to-turn missiles considering their agile dynamics [12–14] and the navigation of skid-to-turn UAVs using camera vision [15] have been investigated. Therefore, in the present study, we describe two new types of path planning algorithms that calculate the paths between two waypoints under constant wind conditions. One type is a rigorous optimization algorithm based on the Euler–Lagrange formulation and the minimum principle with analytical integration of the path. The other type is a fast algorithm describing the path by two circular arcs connected by a line segment or another circular arc in the air mass frame, which is similar to the Dubins path. The latter algorithm is developed for actual airborne application, whereas the former algorithm is developed to check the quasi-optimality of the path calculated by the latter algorithm. We show a convergence proof of the latter algorithm under certain assumptions and its quasi-optimality in comparison with the former algorithm. Furthermore, we seek to demonstrate the computational efficiency and the reliability of the convergence of the latter algorithm through numerical examples.

Kinematics of a Skid-to-Turn UAV

In the present section, the equations describing the kinematics of a skid-to-turn UAV are derived. The variables and coordinate systems in the horizontal plane are shown in Fig. 1. For the sake of simplicity, we assume the following:

1) The motion of the vehicle is constrained in the horizontal plane.

2) The vehicle is turned by side force while maintaining a roll angle of zero.

3) The sideslip angle is sufficiently moderate to prevent directional instability.

4) The rates of change of the velocity and angular velocity components are negligible.

The preceding assumptions are described by the following equations:

$$\dot{\theta} = 0, \quad \alpha = \theta, \quad \phi = 0, \quad |\beta| \ll 1$$
$$\dot{u} = \dot{v} = \dot{w} = \dot{p} = \dot{q} = \dot{r} = 0, \quad V = \text{const} \tag{5}$$

Using these equations, let us approximate the equations of motion. The equations of the angular velocities p, q, and r and the longitudinal velocities u and w are expressed as follows [16]:

$$p = \dot{\phi} - \dot{\psi}\sin\theta = -\dot{\psi}\sin\alpha \tag{6}$$

$$q = \dot{\theta}\cos\phi + \dot{\psi}\sin\phi\cos\theta = 0 \tag{7}$$

$$r = -\dot{\theta}\sin\phi + \dot{\psi}\cos\phi\cos\theta \simeq \dot{\psi}\cos\alpha \tag{8}$$

$$u = V\cos\alpha\cos\beta \simeq V\cos\alpha \tag{9}$$

$$w = V\sin\alpha\cos\beta \simeq V\sin\alpha \tag{10}$$

The differential equations with respect to v and r can be approximated by the following algebraic equations:

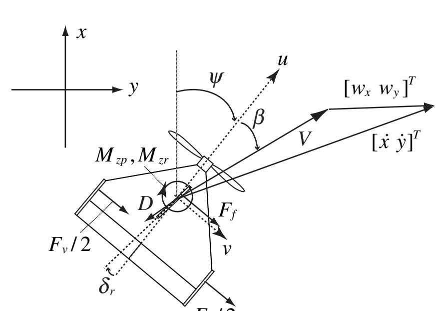

Fig. 1 Variables and coordinate systems in the horizontal plane.

$$\dot{v} = -ru + pw + g\sin\phi\cos\theta + (F_f + F_v - D\sin\beta)/m = 0 \tag{11}$$

$$\dot{r} = \{F_f l_f + F_v l_v + M_{zp} + M_{zr} - (I_{yy} - I_{xx})pq\}/I_{zz} = 0 \tag{12}$$

The forces and moments can be approximated as follows:

$$F_f = c_f\{\delta_r - \beta - \tan^{-1}(l_f r/V)\} \simeq c_f(\delta_r - \beta - l_f\dot{\psi}\cos\alpha/V) \tag{13}$$

$$F_v = -c_v\{\beta + \tan^{-1}(l_v r/V)\} \simeq -c_v(\beta + l_v\dot{\psi}\cos\alpha/V) \tag{14}$$

$$M_{zp} = -c_p p = c_p\dot{\psi}\sin\alpha \tag{15}$$

$$M_{zr} = -c_r r \simeq -c_r\dot{\psi}\cos\alpha \tag{16}$$

Note that the approximations in Eqs. (13) and (14) are based on the additional assumptions $|l_f r/V| \ll 1$ and $|l_v r/V| \ll 1$. Substituting Eqs. (5–10) and (13–16) into Eqs. (11) and (12), and solving them with respect to $\dot{\psi}$ and β, we obtain

$$\dot{\psi} = a_\psi \delta_r \tag{17}$$

$$\beta = a_\beta \delta_r \tag{18}$$

where

$$a_\psi = c_f\{c_v l_v - (c_v + D)l_f\}/a_c \tag{19}$$

$$a_\beta = c_f\{l_f mV + c_v l_v(l_f - l_v)\cos\alpha/V - c_r\cos\alpha + c_p\sin\alpha\}/a_c \tag{20}$$

$$a_c = \{mV + (c_f l_f + c_v l_v)\cos\alpha/V\}(c_f l_f + c_v l_v) - (c_f + c_v + D)[\{(c_f l_f^2 + c_v l_v^2)/V + c_r\}\cos\alpha - c_p\sin\alpha] \tag{21}$$

If the airspeed, the dynamic pressure, and the angle of attack at a specified trim condition are given, then a_ψ and a_β are determined.

On the other hand, the two-dimensional differential equations of the vehicle position are given by

$$\dot{x} = V\cos(\psi + \beta) + w_x \tag{22}$$

$$\dot{y} = V\sin(\psi + \beta) + w_y \tag{23}$$

Substituting Eq. (18) into Eqs. (22) and (23) yields

$$\dot{x} = V\cos(\psi + a_\beta\delta_r) + w_x \tag{24}$$

$$\dot{y} = V\sin(\psi + a_\beta\delta_r) + w_y \tag{25}$$

In addition, the following constraint for the maximum deflection angle of the side-force control surface is enforced:

$$|\delta_r| \le \delta_{r\max} \tag{26}$$

In the path planning algorithms described later herein, Eqs. (17) and (24–26) are adopted as the equations of the kinematics of a skid-to-turn UAV. Because of the term $a_\beta\delta_r$, which appears in the trigonometric functions of Eqs. (24) and (25), the kinematics of the skid-to-turn UAV are different from those of the bank-to-turn UAV [Eqs. (1–4)] (i.e., the direction of the inertial velocity vector $[\dot{x} \quad \dot{y}]^T$ changes instantaneously upon deflection of the side-force control surface δ_r). Thus, the optimal paths of the skid-to-turn UAV are different from Dubins paths. On the other hand, if a_β is set to zero and δ_r and a_ψ are replaced by ϕ and a_ϕ, respectively, then Eqs. (17) and (24–26) are equivalent to Eqs. (1–4). Therefore, the same path planning algorithm can be applied to bank-to-turn vehicles.

In the following sections, we consider the minimum-time path between two waypoints with the kinematics given by Eqs. (17) and (24–26). The boundary conditions at the initial waypoint and the terminal waypoint are given as (x_0, y_0, ψ_0) and (x_f, y_f, ψ_f), respectively. The wind vector $[w_x\ w_y]^T$ is assumed to be constant during the flight between these two waypoints. In this study, we only consider the case in which $\sqrt{w_x^2 + w_y^2} < V$.

Algorithm for Rigorous Calculation of Optimal Path

In this section, the rigorous optimization algorithm is described based on the Euler–Lagrange formulation [17]. The Hamiltonian H of the minimium-time problem is defined by

$$H = 1 + \lambda_x\{V\cos(\psi + a_\beta\delta_r) + w_x\} + \lambda_y\{V\sin(\psi + a_\beta\delta_r) + w_y\} + \lambda_\psi a_\psi\delta_r \tag{27}$$

The differential equations for the adjoints are given as

$$\dot{\lambda}_x = -\frac{\partial H}{\partial x} = 0 \tag{28}$$

$$\dot{\lambda}_y = -\frac{\partial H}{\partial y} = 0 \tag{29}$$

$$\dot{\lambda}_\psi = -\frac{\partial H}{\partial \psi} = \lambda_x V\sin(\psi + a_\beta\delta_r) - \lambda_y V\cos(\psi + a_\beta\delta_r) \tag{30}$$

The condition of the minimum Hamiltonian with regard to the control input is given as follows:

$$\frac{\partial H}{\partial \delta_r} = -\lambda_x V a_\beta\sin(\psi + a_\beta\delta_r) + \lambda_y V a_\beta\cos(\psi + a_\beta\delta_r) + \lambda_\psi a_\psi = 0 \tag{31}$$

$$\frac{\partial^2 H}{\partial \delta_r^2} > 0 \tag{32}$$

If

$$|a_\psi\lambda_\psi/(Va_\beta\sqrt{\lambda_x^2 + \lambda_y^2})| \le 1$$

there is a solution to Eqs. (31) and (32); that is,

$$\bar{\delta}_r = \frac{1}{a_\beta}\left\{-\psi + \tan^{-1}\left(\frac{\lambda_y}{\lambda_x}\right) + \pi - \sin^{-1}\left(\frac{a_\psi\lambda_\psi}{Va_\beta\sqrt{\lambda_x^2 + \lambda_y^2}}\right)\right\} \tag{33}$$

where the range of the arcsine function is $[-\pi/2, \pi/2]$ and that of the arctangent function is chosen such that $\bar{\delta}_r$ is within the range of $[-\pi, \pi]$. Consequently, by invoking the minimum principle [18], the optimal control input is given as

$$\delta_r = \max\{-\delta_{r\max}, \min(\bar{\delta}_r, \delta_{r\max})\}$$

If

$$|a_\psi\lambda_\psi/(Va_\beta\sqrt{\lambda_x^2 + \lambda_y^2})| > 1$$

there is no solution to Eq. (31). In this case, either $-\delta_{r\max}$ or $\delta_{r\max}$, which gives the minimum Hamiltonian, is the optimal control input. To obtain the optimal path, the following boundary conditions must be satisfied:

$$x_e - x_f = 0 \tag{34}$$

$$y_e - y_f = 0 \tag{35}$$

$$\sin\{(\psi_e - \psi_f)/2\} = 0 \tag{36}$$

$$(H)_{t=te} = 1 + \lambda_x\{V\cos(\psi_e + a_\beta\delta_{re}) + w_x\} + \lambda_y\{V\sin(\psi_e + a_\beta\delta_{re}) + w_y\} + \lambda_{\psi e}a_\psi\delta_{re} = 0 \tag{37}$$

Although λ_x and λ_y are time-invariant due to Eqs. (28) and (29), x, y, ψ, and λ_ψ are time-variant. Thus, it is necessary to calculate the time profiles of x, y, ψ, and λ_ψ under three types of control inputs, i.e., unsaturated control ($\delta_r = \bar{\delta}_r$), upper-saturated control ($\delta_r = \delta_{r\max}$), and lower-saturated control ($\delta_r = -\delta_{r\max}$). It is possible to integrate differential Eqs. (17), (24), (25), and (30) analytically by applying any of the three types of control input, and hence the optimal path is described as a set of the following three arcs. We give only the final result of the analytical integrations:

The arc of unsaturated control ($\delta_r = \bar{\delta}_r$) is given as follows:

$$\begin{aligned}x = x_k &- \frac{\lambda_y\lambda_{\psi k}}{\lambda_x^2+\lambda_y^2}\left[\exp\left\{\frac{a_\psi(t-t_k)}{a_\beta}\right\} - 1\right] \\ &- \frac{\lambda_x\lambda_{\psi k}}{(\lambda_x^2+\lambda_y^2)P_k}\left[\sqrt{1 - P_k^2\exp\{\frac{2a_\psi(t-t_k)}{a_\beta}\}} - \sqrt{1-P_k^2}\right] \\ &- \frac{\lambda_x\lambda_{\psi k}}{(\lambda_x^2+\lambda_y^2)P_k}\ln\left[\frac{\sqrt{1-P_k^2}+1}{\sqrt{1-P_k^2\exp\{2a_\psi(t-t_k)/a_\beta\}}+1}\right] \\ &+ \left(-\frac{V\lambda_x}{\sqrt{\lambda_x^2+\lambda_y^2}} + w_x\right)(t-t_k)\end{aligned} \tag{38}$$

$$\begin{aligned}y = y_k &+ \frac{\lambda_x\lambda_{\psi k}}{\lambda_x^2+\lambda_y^2}\left[\exp\left\{\frac{a_\psi(t-t_k)}{a_\beta}\right\} - 1\right] \\ &- \frac{\lambda_y\lambda_{\psi k}}{(\lambda_x^2+\lambda_y^2)P_k}\left[\sqrt{1 - P_k^2\exp\{\frac{2a_\psi(t-t_k)}{a_\beta}\}} - \sqrt{1-P_k^2}\right] \\ &- \frac{\lambda_y\lambda_{\psi k}}{(\lambda_x^2+\lambda_y^2)P_k}\ln\left[\frac{\sqrt{1-P_k^2}+1}{\sqrt{1-P_k^2\exp\{2a_\psi(t-t_k)/a_\beta\}}+1}\right] \\ &+ \left(-\frac{V\lambda_y}{\sqrt{\lambda_x^2+\lambda_y^2}} + w_y\right)(t-t_k)\end{aligned} \tag{39}$$

$$\begin{aligned}\psi = (\psi_k + \sin^{-1}P_k)\exp\left\{-\frac{a_\psi(t-t_k)}{a_\beta}\right\} + \left\{\tan^{-1}\left(\frac{\lambda_y}{\lambda_x}\right) + \pi\right\} \\ \times\left[1 - \exp\left\{-\frac{a_\psi(t-t_k)}{a_\beta}\right\}\right] - \sin^{-1}\left[P_k\exp\left\{\frac{a_\psi(t-t_k)}{a_\beta}\right\}\right] \\ - \frac{P_k[\exp\{-a_\psi(t-t_k)/a_\beta\} - \exp\{a_\psi(t-t_k)/a_\beta\}]}{\sqrt{1-P_k^2\exp\{2a_\psi(t-t_k)/a_\beta\}} + \sqrt{1-P_k^2}}\end{aligned} \tag{40}$$

$$\lambda_\psi = \lambda_{\psi k}\exp\left\{\frac{a_\psi(t-t_k)}{a_\beta}\right\} \tag{41}$$

where

$$P_k = \frac{a_\psi\lambda_{\psi k}}{Va_\beta\sqrt{\lambda_x^2+\lambda_y^2}} \tag{42}$$

The arc of upper-saturated control ($\delta_r = \delta_{r\max}$) is given as follows:

$$\begin{aligned}x = x_k + \frac{V}{a_\psi\delta_{r\max}}[\sin\{\psi_k + a_\beta\delta_{r\max} + a_\psi\delta_{r\max}(t-t_k)\} \\ - \sin(\psi_k + a_\beta\delta_{r\max})] + w_x(t-t_k)\end{aligned} \tag{43}$$

$$\begin{aligned}y = y_k - \frac{V}{a_\psi\delta_{r\max}}[\cos\{\psi_k + a_\beta\delta_{r\max} + a_\psi\delta_{r\max}(t-t_k)\} \\ - \cos(\psi_k + a_\beta\delta_{r\max})] + w_y(t-t_k)\end{aligned} \tag{44}$$

$$\begin{aligned}\lambda_\psi = \lambda_{\psi k} &- \frac{\lambda_x V}{a_\psi\delta_{r\max}}\cos\{\psi_k + a_\beta\delta_{r\max} + a_\psi\delta_{r\max}(t-t_k)\} \\ &- \frac{\lambda_y V}{a_\psi\delta_{r\max}}\sin\{\psi_k + a_\beta\delta_{r\max} + a_\psi\delta_{r\max}(t-t_k)\} \\ &+ \frac{\lambda_x V}{a_\psi\delta_{r\max}}\cos(\psi_k + a_\beta\delta_{r\max}) + \frac{\lambda_y V}{a_\psi\delta_{r\max}}\sin(\psi_k + a_\beta\delta_{r\max})\end{aligned} \tag{45}$$

$$\psi = \psi_k + a_\psi\delta_{r\max}(t-t_k) \tag{46}$$

On the other hand, the arc of lower-saturated control ($\delta_r = -\delta_{r\max}$) can be obtained by replacing $\delta_{r\max}$ in Eqs. (43–46) with $-\delta_{r\max}$.

Switching from one arc to the other arc occurs when either $\bar{\delta}_r = \delta_{r\max}$ or $\bar{\delta}_r = -\delta_{r\max}$ occurs (i.e., when either of the following equations holds):

$$\frac{1}{a_\beta}\left\{-\psi + \tan^{-1}\left(\frac{\lambda_y}{\lambda_x}\right) + \pi - \sin^{-1}\left(\frac{a_\psi\lambda_\psi}{Va_\beta\sqrt{\lambda_x^2+\lambda_y^2}}\right)\right\} = \delta_{r\max} \tag{47}$$

$$\frac{1}{a_\beta}\left\{-\psi + \tan^{-1}\left(\frac{\lambda_y}{\lambda_x}\right) + \pi - \sin^{-1}\left(\frac{a_\psi\lambda_\psi}{Va_\beta\sqrt{\lambda_x^2+\lambda_y^2}}\right)\right\} = -\delta_{r\max} \tag{48}$$

An analytical method by which to obtain the switching time can be described as follows: Here, we present the case of switching from unsaturated control to upper-saturated control. Substituting Eqs. (40) and (41) into Eq. (47), followed by some manipulation, yields

$$\begin{aligned}(1 + a_\beta^2\delta_{r\max}^2)[P_k\exp\{a_\psi(t-t_k)/a_\beta\}]^2 \\ + 2c_1a_\beta\delta_{r\max}[P_k\exp\{a_\psi(t-t_k)/a_\beta\}] + (c_1^2 - 1) = 0\end{aligned} \tag{49}$$

where

$$c_1 \triangleq \sqrt{1-P_k^2} + P_k\{\psi_k + \sin^{-1}P_k - \tan^{-1}(\lambda_y/\lambda_x) - \pi\} \tag{50}$$

From Eq. (49), the switching time t can be calculated as follows:

$$t = t_k + \frac{a_\beta}{a_\psi}\ln\left\{\frac{-c_1a_\beta\delta_{r\max} \pm \sqrt{a_\beta^2\delta_{r\max}^2 - c_1^2 + 1}}{P_k(1 + a_\beta^2\delta_{r\max}^2)}\right\} \tag{51}$$

Note that the valid solution t must satisfy $t_k < t \le t_e$. Similarly, the switching time to lower-saturated control can be obtained by replacing $\delta_{r\max}$ in Eq. (51) with $-\delta_{r\max}$.

Next, we present the case of switching from upper-saturated control to unsaturated control. Substituting Eqs. (45) and (46) into Eq. (47), followed by some manipulation, yields

$$\sqrt{c_2^2 + c_3^2}\sin\{a_\psi \delta_{r\max}(t - t_k) + \tan^{-1}(c_3/c_2)\} = c_4 \tag{52}$$

where

$$\begin{cases} c_2 \triangleq V[a_\beta \delta_{r\max}\sqrt{\lambda_x^2 + \lambda_y^2}\cos\{\psi_k - \tan^{-1}(\lambda_y/\lambda_x) + a_\beta \delta_{r\max}\} - \lambda_x \sin(\psi_k + a_\beta \delta_{r\max}) + \lambda_y \cos(\psi_k + a_\beta \delta_{r\max})] \\ c_3 \triangleq V[a_\beta \delta_{r\max}\sqrt{\lambda_x^2 + \lambda_y^2}\sin\{\psi_k - \tan^{-1}(\lambda_y/\lambda_x) + a_\beta \delta_{r\max}\} + \lambda_x \cos(\psi_k + a_\beta \delta_{r\max}) + \lambda_y \sin(\psi_k + a_\beta \delta_{r\max})] \\ c_4 \triangleq a_\psi \lambda_{\psi k}\delta_{r\max} + \lambda_x V\cos(\psi_k + a_\beta \delta_{r\max}) + \lambda_y V \sin(\psi_k + a_\beta \delta_{r\max}) \end{cases} \tag{53}$$

The solutions to Eq. (52) are given as follows:

$$t = t_k + \frac{1}{a_\psi \delta_{r\max}}\left\{-\tan^{-1}\left(\frac{c_3}{c_2}\right) + \sin^{-1}\left(\frac{c_4}{\sqrt{c_2^2 + c_3^2}}\right)\right\}$$
$$t_k + \frac{1}{a_\psi \delta_{r\max}}\left\{\pi - \tan^{-1}\left(\frac{c_3}{c_2}\right) - \sin^{-1}\left(\frac{c_4}{\sqrt{c_2^2 + c_3^2}}\right)\right\} \tag{54}$$

The valid solution t must satisfy $t_k < t \le t_e$. If both of the solutions satisfy $t_k < t \le t_e$, the smaller solution is the valid solution. The switching time from lower-saturated control to unsaturated control can be similarly obtained by replacing $\delta_{r\max}$ in Eqs. (53) and (54) with $-\delta_{r\max}$.

Based on the arcs and their switching times, as described previously in analytical form, the rigorous path optimization algorithm can be described as follows (see also Fig. 2):

Step 1: Initialize λ_x, λ_y, $\lambda_{\psi 0}$, and t_e.

Step 2: Set $k = 0$ and $t_0 = 0$. Then, if

$$|a_\psi \lambda_{\psi 0}/(V a_\beta \sqrt{\lambda_x^2 + \lambda_y^2})| \le 1$$

calculate $\bar{\delta}_{r0}$ from Eq. (33).

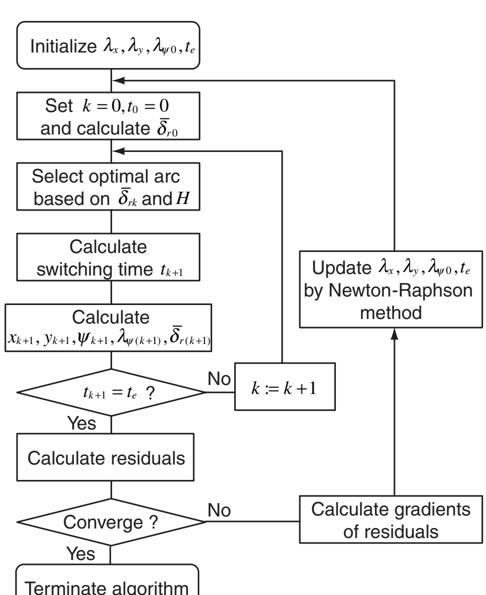

Fig. 2 Flowchart of the rigorous path optimization algorithm.

Step 3: If

$$|a_\psi \lambda_{\psi k}/(V a_\beta \sqrt{\lambda_x^2 + \lambda_y^2})| > 1$$

select the arc of the saturated control that gives minimum H. Otherwise, select the optimal arc based on $\bar{\delta}_{rk}$: If $\bar{\delta}_{rk} \le -\delta_{r\max}$, select the arc of the lower-saturated control. If $\bar{\delta}_{rk} \ge \delta_{r\max}$, select the arc of the upper-saturated control. Otherwise, select the arc of unsaturated control.

Step 4: Calculate the switching time from the current arc to the other arc. If there is no solution to the switching time equations within $(t_k, t_e]$, set $t_{k+1} = t_e$. Otherwise, set t_{k+1} to the calculated switching time.

Step 5: Calculate x_{k+1}, y_{k+1}, ψ_{k+1}, and $\lambda_{\psi(k+1)}$ at $t = t_{k+1}$ of the current arc from the following equations: Eqs. (38–41) in the case of the unsaturated control, Eqs. (43–46) in the case of the upper-saturated control, and Eqs. (43–46), replacing $\delta_{r\max}$ by $-\delta_{r\max}$ in the case of the lower-saturated control. Subsequently, if

$$|a_\psi \lambda_{\psi(k+1)}/(V a_\beta \sqrt{\lambda_x^2 + \lambda_y^2})| \le 1$$

calculate $\bar{\delta}_{r(k+1)}$ at $t = t_{k+1}$ from Eq. (33).

Step 6: If $t_{k+1} = t_e$, go to step 7. Otherwise, increase the index k by one, and return to step 3.

Step 7: Set $x_e = x_{k+1}$, $y_e = y_{k+1}$, $\psi_e = \psi_{k+1}$, $\lambda_{\psi e} = \lambda_{\psi(k+1)}$, and

$$\delta_{re} = \max\{-\delta_{r\max}, \min(\bar{\delta}_{r(k+1)}, \delta_{r\max})\}$$

Then evaluate the residuals of the boundary condition given by Eqs. (34–37).

Step 8: If the residuals are sufficiently small, terminate the algorithm. Otherwise, evaluate the gradients of the residuals with respect to λ_x, λ_y, $\lambda_{\psi 0}$, and t_e, and then update λ_x, λ_y, $\lambda_{\psi 0}$, and t_e by calculating the corrections by the Newton–Raphson method. Then return to step 2.

In the preceding algorithm, given the independent variables λ_x, λ_y, $\lambda_{\psi 0}$, and t_e, the path is analytically integrated and evaluated at the boundary condition. This approach is a type of indirect shooting [19], although indirect shooting usually involves numerical integrations. Because of the analytical integration, the optimal paths calculated by the developed algorithm achieve high accuracy. On the other hand, the convergence of the indirect shooting approach is not robust with respect to the initial guess of the solution [19]. Thus, the algorithm developed in this section is not applicable to the online path planning of UAVs, although it is beneficial for offline use because of its rigorous optimality. However, other optimization approaches, such as direct collocation using fast nonlinear programming [20,21] or a nonlinear receding horizon control approach [22], may be candidates for online path planning due to their relatively stable convergence. Nevertheless, their convergence stabilities are still affected by the initial guesses of the paths. Thus, in the next section, a fast path planning algorithm for which convergence is assured is described.

Algorithm for Fast Calculation of Optimal Path and Proof of Its Convergence

As stated in [8], the path planning problem under constant wind conditions is generally equivalent to finding a path in the air mass frame from an initial position and orientation to a final orientation over a moving virtual target, for which the velocity vector of the virtual target is opposite to the wind vector (see Fig. 3). With respect to constant wind conditions, let us first introduce the following assumption:

Assumption 1: The magnitude of the constant wind vector satisfies $0 < \sqrt{w_x^2 + w_y^2} < V$.

Because the airspeed V is assumed to be constant, the problem is equivalent to finding d such that $T_p(d) - T_{vt}(d) = 0$, where $T_{vt}(d)$ can be described as

$$T_{vt}(d) = d/\sqrt{w_x^2 + w_y^2} \tag{55}$$

Moreover, the terminal condition for the path in the air mass frame is then specified as

$$(\tilde{x}_e, \tilde{y}_e, \psi_e) = (x_f - w_x T_{vt}(d), y_f - w_y T_{vt}(d), \psi_f) \tag{56}$$

Let the subscripts for R, L, and S be the length of the arc or the line segment. Then let us consider the following proposition:

Proposition 1: For any boundary conditions and wind vector satisfying Assumption 1, at least one of the following paths,

$$\{RSR, LSL, RSL, LSR, RL_\sigma R, RL_\xi R, LR_\sigma L, LR_\xi L\}$$

where $\pi\rho \le \sigma \le 2\pi\rho$ and $0 \le \xi \le \pi\rho$, can intercept the virtual target in the air mass frame.

Proposition 1 is a basis for the fast path calculation algorithm described later. The set of paths covered in Proposition 1 is similar to that proposed in [8], which consists of six types of Dubins paths and two types of non-Dubins paths. However, unlike the paths in [8], the arcs and the line segments constituting the paths in Proposition 1 intersect at an angle $\hat{\beta}$, as shown in Fig. 4. This is due to the kinematics described by Eqs. (24) and (25), which imply that the direction of the inertial velocity vector $[\dot{x}\ \dot{y}]^T$ changes instantaneously upon deflection of the side-force control surface.

As the bases of a proof of Proposition 1, we present several lemmas and their proofs. Some of the lemmas are extensions of the properties of the paths proved in [8] to those of the eight paths defined in Proposition 1.

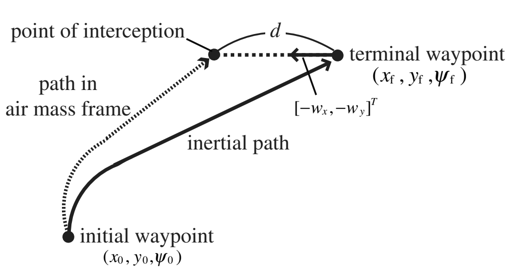

Fig. 3 Equivalent problem of interception in the air mass frame.

Lemma 1: $RL_\sigma R$ and $RL_\xi R$ ($\pi\rho \le \sigma \le 2\pi\rho$ and $0 \le \xi \le \pi\rho$) exist if

$$\sqrt{(a_{fr} - a_{0r})^2 + (b_{fr} - b_{0r})^2} \le 4\rho\cos\hat{\beta}$$

and $LR_\sigma L$ and $LR_\xi L$ ($\pi\rho \le \sigma \le 2\pi\rho$, $0 \le \xi \le \pi\rho$) exist if

$$\sqrt{(a_{fl} - a_{0l})^2 + (b_{fl} - b_{0l})^2} \le 4\rho\cos\hat{\beta}$$

At each boundary, $RL_\sigma R = RL_\xi R = RL_{\pi\rho} R$ or $LR_\sigma L = LR_\xi L = LR_{\pi\rho} L$ holds.

Proof: Let us consider the case of $RL_\sigma R$ and $RL_\xi R$. The following equations for (a_{ml}, b_{ml}) (i.e., the center of the middle circular arc) hold geometrically:

$$(a_{ml} - a_{0r})^2 + (b_{ml} - b_{0r})^2 = 4\rho^2\cos^2\hat{\beta} \tag{57}$$

$$(a_{ml} - a_{fr})^2 + (b_{ml} - b_{fr})^2 = 4\rho^2\cos^2\hat{\beta} \tag{58}$$

By eliminating b_{ml} from Eqs. (57) and (58), we obtain a quadratic equation in a_{ml}, as follows:

$$\begin{aligned}&\{(a_{fr} - a_{0r})^2 + (b_{fr} - b_{0r})^2\}a_{ml}^2 - \{(a_{fr} - a_{0r})^2 \\ &\quad + (b_{fr} - b_{0r})^2\}(a_{fr} + a_{0r})a_{ml} + \{(a_{fr} + a_{0r})^2(a_{fr} - a_{0r})^2 \\ &\quad + 2(a_{fr}^2 + a_{0r}^2)(b_{fr} - b_{0r})^2 + (b_{fr} - b_{0r})^4\}/4 \\ &\quad - 4\rho^2\cos^2\hat{\beta}(b_{fr} - b_{0r})^2 = 0\end{aligned} \tag{59}$$

From the discriminant of Eq. (59), the necessary and sufficient condition for the existence of a_{ml} and b_{ml}, which is equivalent to the existence of $RL_\sigma R$ and $RL_\xi R$, is

$$\sqrt{(a_{fr} - a_{0r})^2 + (b_{fr} - b_{0r})^2} \le 4\rho\cos\hat{\beta}$$

In the case of

$$\sqrt{(a_{fr} - a_{0r})^2 + (b_{fr} - b_{0r})^2} < 4\rho\cos\hat{\beta}$$

there are two pairs of solutions to Eqs. (57) and (58), which correspond to the centers of the second circular arcs in $RL_\sigma R$ and $RL_\xi R$. In the case of

$$\sqrt{(a_{fr} - a_{0r})^2 + (b_{fr} - b_{0r})^2} = 4\rho\cos\hat{\beta}$$

there is a unique solution to Eqs. (57) and (58), which corresponds to the boundary case: $RL_\sigma R = RL_\xi R = RL_{\pi\rho} R$. By permuting R and L, the same arguments hold for $LR_\sigma L$ and $LR_\xi L$.

Lemma 2: RSL exists if

$$\sqrt{(a_{fl} - a_{0r})^2 + (b_{fl} - b_{0r})^2} \ge 2\rho\cos\hat{\beta}$$

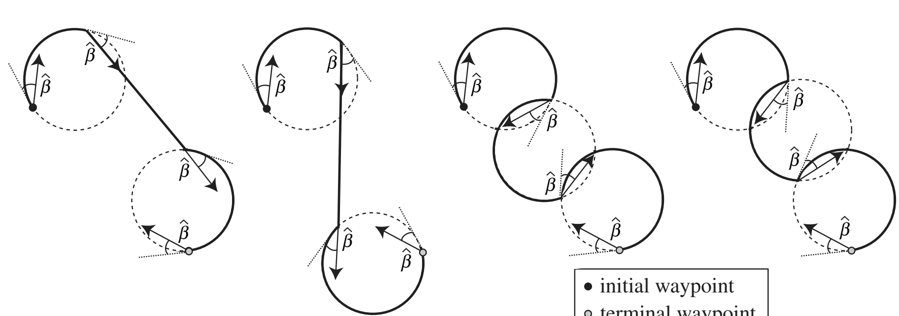

Fig. 4 Examples of paths of the fast algorithm (RSR, RSL, $RL_\sigma R$, and $RL_\xi R$).

and LSR exists if

$$\sqrt{(a_{fr}-a_{0l})^2+(b_{fr}-b_{0l})^2} \geq 2\rho\cos\hat{\beta}$$

At each boundary, $RSL = RS_0L$ or $LSR = LS_0R$ holds.

Proof: Let us consider the case of RSL. The intersection point $(\tilde{x}_{c1}, \tilde{y}_{c1})$ between R and S geometrically satisfies the following equations:

$$(\tilde{x}_{c1}-a_{0r})^2+(\tilde{y}_{c1}-b_{0r})^2=\rho^2 \tag{60}$$

$$\begin{aligned}(\tilde{x}_{c1}-a_{0r})\{\tilde{x}_{c1}-(a_{0r}+a_{fl})/2\}+(\tilde{y}_{c1}-b_{0r})\{\tilde{y}_{c1}\\ -(b_{0r}+b_{fl})/2\}-\tan\hat{\beta}[\{\tilde{x}_{c1}-(a_{0r}+a_{fl})/2\}(\tilde{y}_{c1}-b_{0r})\\ -\{\tilde{y}_{c1}-(b_{0r}+b_{fl})/2\}(\tilde{x}_{c1}-a_{0r})]=0\end{aligned} \tag{61}$$

By eliminating $\tilde{y}_{c1}$ from Eqs. (60) and (61), we obtain a quadratic equation in $\tilde{x}_{c1}$ as follows:

$$(\zeta_0^2+\eta_0^2)(\tilde{x}_{c1}-a_{0r})^2-2\rho^2\eta_0(\tilde{x}_{c1}-a_{0r})+\rho^2(\rho^2-\zeta_0^2)=0 \tag{62}$$

where

$$\begin{aligned}\zeta_0 &\triangleq \{(b_{fl}-b_{0r})-\tan\hat{\beta}(a_{fl}-a_{0r})\}/2\\ \eta_0 &\triangleq \{(a_{fl}-a_{0r})+\tan\hat{\beta}(b_{fl}-b_{0r})\}/2\end{aligned} \tag{63}$$

From the discriminant of Eq. (62), the necessary and sufficient condition for the existence of $(\tilde{x}_{c1}, \tilde{y}_{c1})$ is

$$\sqrt{(a_{fl}-a_{0r})^2+(b_{fl}-b_{0r})^2} \geq 2\rho\cos\hat{\beta}$$

The valid solution to Eq. (62) is given as follows:

$$\begin{aligned}\tilde{x}_{c1} &= a_{0r}+\rho\cdot\frac{\rho\eta_0+\zeta_0\sqrt{\zeta_0^2+\eta_0^2-\rho^2}}{\zeta_0^2+\eta_0^2}\\ \tilde{y}_{c1} &= b_{0r}+\rho\cdot\frac{\rho\zeta_0-\eta_0\sqrt{\zeta_0^2+\eta_0^2-\rho^2}}{\zeta_0^2+\eta_0^2}\end{aligned} \tag{64}$$

Similar arguments hold for $(\tilde{x}_{c2}, \tilde{y}_{c2})$, which is the intersection point of S and L on RSL; the necessary and sufficient condition for the existence of $(\tilde{x}_{c2}, \tilde{y}_{c2})$ is

$$\sqrt{(a_{fl}-a_{0r})^2+(b_{fl}-b_{0r})^2} \geq 2\rho\cos\hat{\beta}$$

and the valid point $(\tilde{x}_{c2}, \tilde{y}_{c2})$ is given as follows:

$$\begin{aligned}\tilde{x}_{c2} &= a_{fl}+\rho\cdot\frac{\rho\eta_f+\zeta_f\sqrt{\zeta_f^2+\eta_f^2-\rho^2}}{\zeta_f^2+\eta_f^2}\\ \tilde{y}_{c2} &= b_{fl}+\rho\cdot\frac{\rho\zeta_f-\eta_f\sqrt{\zeta_f^2+\eta_f^2-\rho^2}}{\zeta_f^2+\eta_f^2}\end{aligned} \tag{65}$$

where

$$\begin{aligned}\zeta_f &\triangleq \{(b_{0r}-b_{fl})+\tan\hat{\beta}(a_{0r}-a_{fl})\}/2\\ \eta_f &\triangleq \{(a_{0r}-a_{fl})-\tan\hat{\beta}(b_{0r}-b_{fl})\}/2\end{aligned} \tag{66}$$

Because the existence of both $(\tilde{x}_{c1}, \tilde{y}_{c1})$ and $(\tilde{x}_{c2}, \tilde{y}_{c2})$ are equivalent to the existence of RSL, the necessary and sufficient condition for the existence of RSL is

$$\sqrt{(a_{fl}-a_{0r})^2+(b_{fl}-b_{0r})^2} \geq 2\rho\cos\hat{\beta}$$

On the other hand, it is trivial to show that $\zeta_0^2+\eta_0^2=\zeta_f^2+\eta_f^2=\rho^2$ holds if

$$\sqrt{(a_{fl}-a_{0r})^2+(b_{fl}-b_{0r})^2} = 2\rho\cos\hat{\beta}$$

In this case, the length of S, which is given by

$$\sqrt{(\tilde{x}_{c2}-\tilde{x}_{c1})^2+(\tilde{y}_{c2}-\tilde{y}_{c1})^2}$$

becomes zero. Consequently, $RSL = RS_0L$ holds at the boundary. By permuting R and L, the same arguments hold for LSR.

Lemma 3: If

$$\sqrt{(a_{fr}-a_{0r})^2+(b_{fr}-b_{0r})^2} = 4\rho\cos\hat{\beta}$$

at least one of the paths in the set $\{RSR, LSL, RSL, LSR, LR_\sigma L\}$ $(\pi\rho \leq \sigma \leq 2\pi\rho)$ is shorter than $RL_{\pi\rho}R$. If

$$\sqrt{(a_{fl}-a_{0l})^2+(b_{fl}-b_{0l})^2} = 4\rho\cos\hat{\beta}$$

at least one of the paths in $\{RSR, LSL, RSL, LSR, RL_\sigma R\}$ is shorter than $LR_{\pi\rho}L$.

Proof: Consider the case of

$$\sqrt{(a_{fr}-a_{0r})^2+(b_{fr}-b_{0r})^2} = 4\rho\cos\hat{\beta}$$

Without loss of generality, it is possible to choose $(a_{0r}, b_{0r}) = (0, 0)$ and $(a_{fr}, b_{fr}) = (4\rho\cos\hat{\beta}, 0)$. Then, by introducing χ_0 and χ_f, as illustrated in Fig. 5,

$$(a_{0l}, b_{0l}) = (2\rho\cos\hat{\beta}\cos\chi_0, 2\rho\cos\hat{\beta}\sin\chi_0)$$

and

$$(a_{fl}, b_{fl}) = (4\rho\cos\hat{\beta}+2\rho\cos\hat{\beta}\cos\chi_f, 2\rho\cos\hat{\beta}\sin\chi_f)$$

hold. Note that χ_0 and χ_f are independent of $\hat{\beta}$ and are given as $\chi_0 = \psi_0 - \pi/2$ and $\chi_f = \psi_f - \pi/2$, respectively. The length of each path can then be calculated as follows:

$$l(RL_{\pi\rho}R) = \rho\{M(2\pi-\chi_0)+\pi+M(\chi_f-\pi)\} \tag{67}$$

$$l(RSR) = \rho\{M(3\pi/2-\chi_0)+4\cos\hat{\beta}+M(\chi_f-3\pi/2)\} \tag{68}$$

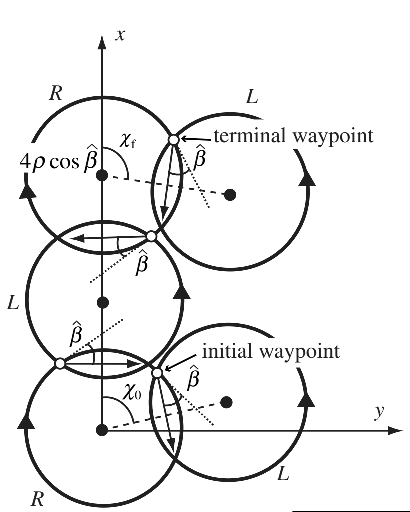

Fig. 5 Circular arcs in the case of $\sqrt{(a_{fr}-a_{0r})^2+b_{fr}-b_{0r})^2} = 4\rho\cos\hat{\beta}$.

$$l(RSL) = \rho\{M(\chi_{m1} - \chi_0) + 4\cos\hat{\beta}\sqrt{1+\cos\chi_f} + M(\chi_{m1} - \pi - \chi_f)\} \tag{69}$$

$$l(LSR) = \rho\{M(\chi_0 + \pi - \chi_{m2}) + 4\cos\hat{\beta}\sqrt{1-\cos\chi_0} + M(\chi_f - \chi_{m2} - \pi)\} \tag{70}$$

$$l(LSL) = \rho\{M(\chi_0 + \pi - \chi_{m3}) + 2\cos\hat{\beta}\sqrt{6 - 2\cos(\chi_f - \chi_0) + 4\cos\chi_f - 4\cos\chi_0} + M(\chi_{m3} - \chi_f)\} \tag{71}$$

$$l(LRL) = \rho\{M(\chi_0 + \pi - \chi_{m4}) + M(\chi_{m5} - \chi_{m4}) + M(\chi_{m5} + \pi - \chi_f)\} \tag{72}$$

where

$$\chi_{m1} \triangleq \tan^{-1}\left(\frac{\sin\chi_f}{2+\cos\chi_f}\right) - \cos^{-1}\left(\frac{1}{\sqrt{5+4\cos\chi_f}}\right) \tag{73}$$

$$\chi_{m2} \triangleq -\tan^{-1}\left(\frac{\sin\chi_0}{2-\cos\chi_0}\right) + \cos^{-1}\left(\frac{1}{\sqrt{5-4\cos\chi_0}}\right) \tag{74}$$

$$\chi_{m3} \triangleq \tan^{-1}\left(\frac{\sin\chi_f - \sin\chi_0}{2+\cos\chi_f - \cos\chi_0}\right) - \frac{\pi}{2} \tag{75}$$

$$\chi_{m4} \triangleq \tan^{-1}[\{(\sin\chi_f - \sin\chi_0) \mp (2+\cos\chi_f - \cos\chi_0)\gamma\}/\{(2+\cos\chi_f - \cos\chi_0) \pm (\sin\chi_f - \sin\chi_0)\gamma\}] \tag{76}$$

$$\chi_{m5} \triangleq \tan^{-1}[\{(\sin\chi_0 - \sin\chi_f) \mp (2+\cos\chi_f - \cos\chi_0)\gamma\}/\{(\cos\chi_0 - 2 - \cos\chi_f) \pm (\sin\chi_f - \sin\chi_0)\gamma\}] \tag{77}$$

$$\gamma = \sqrt{\frac{1}{6 - 2\cos(\chi_f - \chi_0) + 4\cos\chi_f - 4\cos\chi_0} - \frac{1}{4}} \tag{78}$$

Note that $\chi_{m1}, \ldots, \chi_{m5}$ are independent of $\hat{\beta}$. Because $l(RL_{\pi\rho}R)$, $l(RSR)|_{\hat{\beta}=0}$, $l(RSL)|_{\hat{\beta}=0}$, $l(LSR)|_{\hat{\beta}=0}$, $l(LSL)|_{\hat{\beta}=0}$, and $l(LRL)$ are independent of $\hat{\beta}$, the problem of finding the shortest length among these is equivalent to finding the shortest Dubins path. In [6], it was proven that $RL_{\pi\rho}R$ cannot be the shortest Dubins path. Hence, at least one of

$$\{l(RSR)|_{\hat{\beta}=0}, l(RSL)|_{\hat{\beta}=0}, l(LSR)|_{\hat{\beta}=0}, l(LSL)|_{\hat{\beta}=0}, l(LRL)\}$$

is shorter than $l(RL_{\pi\rho}R)$. In addition, $l(RSR) \le l(RSR)|_{\hat{\beta}=0}$, $l(RSL) \le l(RSL)|_{\hat{\beta}=0}$, $l(LSR) \le l(LSR)|_{\hat{\beta}=0}$, and $l(LSL) \le l(LSL)|_{\hat{\beta}=0}$ hold, because $|\hat{\beta}| \ll 1$. Therefore, at least one of

$$\{l(RSR), l(RSL), l(LSR), l(LSL), l(LRL)\}$$

is shorter than $D(RL_{\pi\rho}R)$. By permuting R and L, the same arguments hold for the case of

$$\sqrt{(a_{fl} - a_{0l})^2 + (b_{fl} - b_{0l})^2} = 4\rho\cos\hat{\beta}$$

Lemma 4: $T_p(0) - T_{vt}(0) \ge 0$ holds. In addition, $T_p(d) - T_{vt}(d) < 0$ holds for sufficiently large d.

Proof: From Eq. (55), $T_{vt}(0) = 0$ holds. If $(x_0, y_0, \psi_0) \ne (x_f, y_f, \psi_f)$, a positive finite time is required for the vehicle to change its state from (x_0, y_0, ψ_0) to

$$(x_f - w_x T_{vt}(0), y_f - w_y T_{vt}(0), \psi_f) = (x_f, y_f, \psi_f)$$

in the air mass frame [i.e., $T_p(0) > 0$ holds]. If $(x_0, y_0, \psi_0) = (x_f, y_f, \psi_f)$, then $T_p(0) = 0$ holds. Therefore, $T_p(0) - T_{vt}(0) = T_p(0) \ge 0$ holds. On the other hand, if d is sufficiently large, neither

$$\sqrt{(a_{fr} - a_{0r})^2 + (b_{fr} - b_{0r})^2} \le 4\rho\cos\hat{\beta}$$

nor

$$\sqrt{(a_{fl} - a_{0l})^2 + (b_{fl} - b_{0l})^2} \le 4\rho\cos\hat{\beta}$$

hold. Then, from Lemma 1, only *RSR*, *LSL*, *RSL*, and *LSR* exist among the eight candidate paths. As d becomes larger, the length of the line segment S accounts for the majority of the length of each of the four paths. In other words, $T_p(d)$ of each of the four paths approaches d/V as d becomes larger. From Eq. (55) and Assumption 1,

$$T_{vt}(d) = d/\sqrt{w_x^2 + w_y^2} > d/V$$

Consequently, $T_p(d) - T_{vt}(d) < 0$ holds for sufficiently large d.

Lemma 5: The length of the shortest path chosen from the set

$$\{RSR, LSL, RSL, LSR, RL_\sigma R, RL_\xi R, LR_\sigma L, LR_\xi L\}$$

is continuous with respect to d, except at the boundary of the existence of *RSL* or *LSR*: that is,

$$\sqrt{(a_{fl} - a_{0r})^2 + (b_{fl} - b_{0r})^2} = 2\rho\cos\hat{\beta}$$

or

$$\sqrt{(a_{fr} - a_{0l})^2 + (b_{fr} - b_{0l})^2} = 2\rho\cos\hat{\beta}$$

Proof: Discontinuities of each path may occur 1) at the singular points at which the path includes any of R_0, L_0, $R_{2\pi\rho}$, $L_{2\pi\rho}$, and S_0 or 2) at the boundaries of the path existence described by Lemmas 1 and 2. At the singular points corresponding to R_0SR, RSR_0, R_0SL, LSR_0, RS_0R, and RL_0R, the shortest path type changes in the following manner as d increases:

1) $R_\varepsilon SR \to R_0SR \sim L_0SR \to L_\varepsilon SR$.
2) $RSR_{\varepsilon0} \to RSR_0 \sim RSL_0 \to RSL_{\varepsilon0}$.
3) $R_\varepsilon SL \to R_0SL \sim L_0SL \to L_\varepsilon SL$.
4) $LSR_\varepsilon \to LSR_0 \sim LSL_0 \to LSL_\varepsilon$.
5) $RS_{\varepsilon1}R \to R_\mu S_0 R_\nu \sim L_0 R_{\mu+\nu} L_0 \to L_{\varepsilon2} R_{\mu+\nu+\varepsilon4} L_{\varepsilon3}$.
6) $RL_{\varepsilon1}R \to R_\mu L_0 R_\nu \sim L_0 R_{\mu+\nu} L_0 \to L_{\varepsilon2} R_{\mu+\nu+\varepsilon4} L_{\varepsilon3}$.

where the notation $\to$ denotes a slight change in the length of the selected path in concert with a slight increase in d, and the notation $\sim$ denotes a change in the selected path to another path of the same length. As an example, the change in the path types in item 2 is shown in Fig. 6. Thus, the discontinuity of the shortest path length at these singular points does not occur. In addition, the shortest path does not encounter the singular points corresponding to $R_{2\pi\rho}SR$, $RSR_{2\pi\rho}$, $R_{2\pi\rho}SL$, $LSR_{2\pi\rho}$, or $RL_{2\pi\rho}R$. This is because these paths can be shortened further by replacing $R_{2\pi\rho}$ or $L_{2\pi\rho}$ with R_0 or L_0,

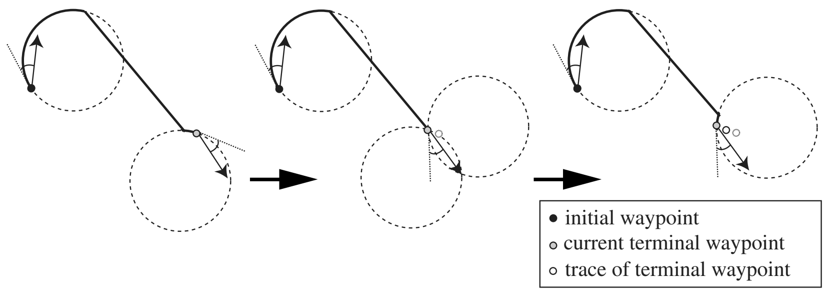

Fig. 6 Example of the change of path type from RSR to RSL as *d* increases.

respectively, and, based on items 1–4 and 6, these shortened paths change continuously as d increases. By permuting R and L of the preceding arguments, the discontinuity of the shortest path can be confirmed to not occur at the singular points corresponding to L_0SL, LSL_0, L_0SR, RSL_0, LS_0L, LR_0L, $L_{2\pi\rho}SL$, $LSL_{2\pi\rho}$, $L_{2\pi\rho}SR$, $RSL_{2\pi\rho}$, or $LR_{2\pi\rho}L$. Moreover, from Lemmas 1 and 3, neither $RL_{\pi\rho}R$ nor $LR_{\pi\rho}L$, which exist in the case of

$$\sqrt{(a_{fr}-a_{0r})^2+(b_{fr}-b_{0r})^2}=4\rho\cos\hat{\beta}$$

or

$$\sqrt{(a_{fl}-a_{0l})^2+(b_{fl}-b_{0l})^2}=4\rho\cos\hat{\beta}$$

is the shortest path. Therefore, discontinuity of the shortest path at these boundaries does not occur. On the other hand,

$$\sqrt{(a_{fl}-a_{0r})^2+(b_{fl}-b_{0r})^2}=2\rho\cos\hat{\beta}$$

or

$$\sqrt{(a_{fr}-a_{0l})^2+(b_{fr}-b_{0l})^2}=2\rho\cos\hat{\beta}$$

holds at the singular points corresponding to R_0LR, RLR_0, L_0RL, LRL_0, $R_{2\pi\rho}LR$, $RLR_{2\pi\rho}$, $L_{2\pi\rho}RL$, and $LRL_{2\pi\rho}$ as well as RS_0L and LS_0R. In these cases, feasible path changes, such as items 1–6, do not necessarily exist, and hence discontinuities may occur.

Lemma 6: Let us consider the case in which the sequence of the shortest paths with d increasing from zero passes through either

$$\sqrt{(a_{fl}-a_{0r})^2+(b_{fl}-b_{0r})^2}=2\rho\cos\hat{\beta}$$

or

$$\sqrt{(a_{fr}-a_{0l})^2+(b_{fr}-b_{0l})^2}=2\rho\cos\hat{\beta}$$

and the following discontinuity occurs: $T_p(d)-T_{vt}(d)>0$ before passing the boundary and $T_p(d)-T_{vt}(d)<0$ after passing the boundary. In this case, one of the paths in the set $\{RL_\sigma R, RL_\xi R, LR_\sigma L, LR_\xi L\}$ satisfies $T_p(d)-T_{vt}(d)=0$ at some d.

Proof: Let us consider the case of

$$\sqrt{(a_{fl}-a_{0r})^2+(b_{fl}-b_{0r})^2}=2\rho\cos\hat{\beta}$$

Before passing the boundary, $T_p(d)-T_{vt}(d)>0$ holds in the cases of both $RL_\sigma R$ and $RL_\xi R$. After passing the boundary, $T_p(d)-T_{vt}(d)<0$ holds in the case of either $RL_\xi R_0$ or $RL_\sigma R_0$ because the discontinuous decrease of the length will occur in either one of the two paths (i.e., $RL_\xi R_{2\pi\rho}\to RL_{\xi+\varepsilon}R_0$ or $RL_\sigma R_{2\pi\rho}\to RL_{\sigma+\varepsilon}R_0$). On the other hand, $T_p(d)-T_{vt}(d)>0$ still holds in the rest of the paths after passing the boundary. As d increases further, $RL_\xi R$ and $RL_\sigma R$ become identical (i.e., $RL_{\pi\rho}R$) at

$$\sqrt{(a_{fr}-a_{0r})^2+(b_{fr}-b_{0r})^2}=4\rho\cos\hat{\beta}$$

This signifies that $T_p(d)-T_{vt}(d)$ of either $RL_\xi R$ or $RL_\sigma R$ crosses zero. By permuting R and L of the preceding arguments, $T_p(d)-T_{vt}(d)$ of either $LR_\xi L$ or $LR_\sigma L$ crosses zero when

$$\sqrt{(a_{fr}-a_{0l})^2+(b_{fr}-b_{0l})^2}=2\rho\cos\hat{\beta}$$

Based on the preceding lemmas, the proof of Proposition 1 can be given as follows:

Proof of Proposition 1: From Lemma 5, if the sequence of the shortest paths in the set

$$\{RSR, LSL, RSL, LSR, RL_\sigma R, RL_\xi R, LR_\sigma L, LR_\xi L\}$$

passes through neither

$$\sqrt{(a_{fl}-a_{0r})^2+(b_{fl}-b_{0r})^2}=2\rho\cos\hat{\beta}$$

nor

$$\sqrt{(a_{fr}-a_{0l})^2+(b_{fr}-b_{0l})^2}=2\rho\cos\hat{\beta}$$

then $T_p(d)-T_{vt}(d)$ is continuous. Then, from Lemma 3, the shortest path satisfies $T_p(d)-T_{vt}(d)=0$ at some d. If the sequence of the shortest paths passes through

$$\sqrt{(a_{fl}-a_{0r})^2+(b_{fl}-b_{0r})^2}=2\rho\cos\hat{\beta}$$

or

$$\sqrt{(a_{fr}-a_{0l})^2+(b_{fr}-b_{0l})^2}=2\rho\cos\hat{\beta}$$

and $T_p(d)-T_{vt}(d)>0$ holds in the shortest path after passing the boundary, the shortest path still satisfies $T_p(d)-T_{vt}(d)=0$ at some d due to the continuity of the subsequent sequence of the shortest paths. If the case considered in Lemma 6 occurs, one of the paths in the set $\{RL_\sigma R, RL_\xi R, LR_\sigma L, LR_\xi L\}$ (which is not necessarily the shortest path) satisfies $T_p(d)-T_{vt}(d)=0$ at some d. Therefore, at least one of the paths in the set

$$\{RSR, LSL, RSL, LSR, RL_\sigma R, RL_\xi R, LR_\sigma L, LR_\xi L\}$$

satisfies $T_p(d)-T_{vt}(d)=0$ at some d, and hence the interception of the virtual target is achieved.

Although the preceding discussion does not cover the case in which $\sqrt{w_x^2+w_y^2}=0$ (the no-wind case) due to Assumption 1, the eight candidate inertial paths in this case can be readily calculated without considering the interception problem ($T_p(d)-T_{vt}(d)=0$). The fast path calculation algorithm can then be described as follows:

Step 1: If $0<\sqrt{w_x^2+w_y^2}<V$, find the minimum root of $\{T_p(d)-T_{vt}(d)=0, d\geq 0\}$ with respect to each of the eight candidate air mass frame paths:

$$\{RSR, LSL, RSL, LSR, RL_\sigma R, RL_\xi R, LR_\sigma L, LR_\xi L\}$$

where $\pi\rho \leq \sigma \leq 2\pi\rho$, $0 \leq \xi \leq \pi\rho$. In our implementation, the algorithm by Brent [23] is adopted for finding the root. If $\sqrt{w_x^2 + w_y^2} = 0$, find the shortest of the eight candidate inertial paths and terminate the algorithm.

Step 2: Choose the minimum root among those found in step 1 and the corresponding path type.

Step 3: Modify the path chosen in step 2 by a transformation from the air mass frame $(\tilde{x}(t), \tilde{y}(t))$ to the inertial frame $(x(t), y(t))$ as follows:

$$x(t) = \tilde{x}(t) + w_x t, y(t) = \tilde{y}(t) + w_y t \tag{79}$$

Then terminate the algorithm.

The convergence of the algorithm is guaranteed because Proposition 1 guarantees that at least one of the eight root-finding processes carried out in step 1 will find a solution. Note that the domains of d are bounded for some paths. For clarity, let $(a_{fr}(0), b_{fr}(0))$ and $(a_{fl}(0), b_{fl}(0))$ be the centers of the terminal circular arcs at $d = 0$. The condition of the existence of RSL can be described as follows:

$$\sqrt{\left(a_{fl}(0) - \frac{w_x d}{\sqrt{w_x^2 + w_y^2}} - a_{0r}\right)^2 + \left(b_{fl}(0) - \frac{w_y d}{\sqrt{w_x^2 + w_y^2}} - b_{0r}\right)^2} \leq 2\rho \cos\hat{\beta} \tag{80}$$

This is equivalent to the following quadratic inequality:

$$d^2 - 2\{w_x(a_{fl}(0) - a_{0r}) + w_y(b_{fl}(0) - b_{0r})\}d/\sqrt{w_x^2 + w_y^2} + \{(a_{fl}(0) - a_{0r})^2 + (b_{fl}(0) - b_{0r}) - 4\rho^2\cos^2\hat{\beta}\} \geq 0 \tag{81}$$

If the discriminant of the left-hand side of Eq. (81) is less than or equal to zero, the domain for finding the root is $d \geq 0$. Otherwise, the domain for finding the root is the solution to Eq. (80) and $d \geq 0$. Similarly, the condition of the existence of $RL_\sigma R$ and $RL_\xi R$ can be described by the following inequality:

$$d^2 - 2\{w_x(a_{fr}(0) - a_{0r}) + w_y(b_{fr}(0) - b_{0r})\}d/\sqrt{w_x^2 + w_y^2} + \{(a_{fr}(0) - a_{0r})^2 + (b_{fr}(0) - b_{0r}) - 16\rho^2\cos^2\hat{\beta}\} \leq 0 \tag{82}$$

Then the domain for finding the root is the solution to Eq. (82) and $d \geq 0$. By permuting R and L, the same arguments hold for LSR, $LR_\sigma L$, and $LR_\xi L$.

Numerical Examples

Because the fast algorithm described in the previous section has guaranteed convergence under certain assumptions, it may be applicable to online path planning for airborne application if the computational speed is practical. However, the paths calculated by the fast algorithm are achieved by bang–bang controls, whereas the optimal paths calculated by the rigorous algorithm are generally achieved by continuous controls. Thus, in this section, the quality and the computational speed of the fast algorithm, together with the reliability of the convergence, are examined through numerical examples. The performance parameters in the path planning are $V = 10$ m/s, $a_\psi = 1$ 1/s, $a_\beta = -1$, and $\delta_{r\,\max} = \pi/18$ rad; these values, determined arbitrarily, are used in all the numerical simulations.

First, we consider the following four sets of boundary conditions and wind vectors.

Case 1: $(x_0, y_0, \psi_0) = (0, 0, 0)$, $(x_f, y_f, \psi_f) = (100, 0, 0)$, $[w_x\ w_y]^T = [0\ -5]^T$

Case 2: $(x_0, y_0, \psi_0) = (0, 0, 0)$, $(x_f, y_f, \psi_f) = (100, 0, 0)$, $[w_x\ w_y]^T = [0\ -3]^T$

Case 3: $(x_0, y_0, \psi_0) = (0, 0, 0)$, $(x_f, y_f, \psi_f) = (100, 100, \pi/2)$, $[w_x\ w_y]^T = [-2\ -0]^T$

Case 4: $(x_0, y_0, \psi_0) = (0, 0, 0)$, $(x_f, y_f, \psi_f) = (100, -100, -\pi/4)$, $[w_x\ w_y]^T = [-2\ -4]^T$

Both the fast algorithm and the rigorous algorithm were run for each case. It took some time and effort to calculate the optimal paths by the rigorous algorithm, because initial guesses of λ_x, λ_y, $\lambda_{\psi 0}$, and t_e were given by trial and error. The paths calculated by both algorithms are shown in Figs. 7–10. The types of the resulting paths calculated by the fast algorithm were $RL_\sigma R$ in case 1, RSL in case 2, RSR in case 3, and $LR_\xi L$ in case 4. Symmetric changes of both the terminal conditions and the wind vectors with respect to the x axis in these cases would produce the path types $LR_\sigma L$, LSR, LSL, and $RL_\xi R$. Thus, it can be confirmed that each of the eight candidate paths in Proposition 1 can be adopted in the running of the fast algorithm. Table 1 shows the total elapsed times of the paths as well as the differences between these times. As shown in Figs. 7–9, the time histories of δ_r for the fast algorithm approximated those of the rigorous algorithm. In these cases, the differences in elapsed times between the fast algorithm and the rigorous algorithm were

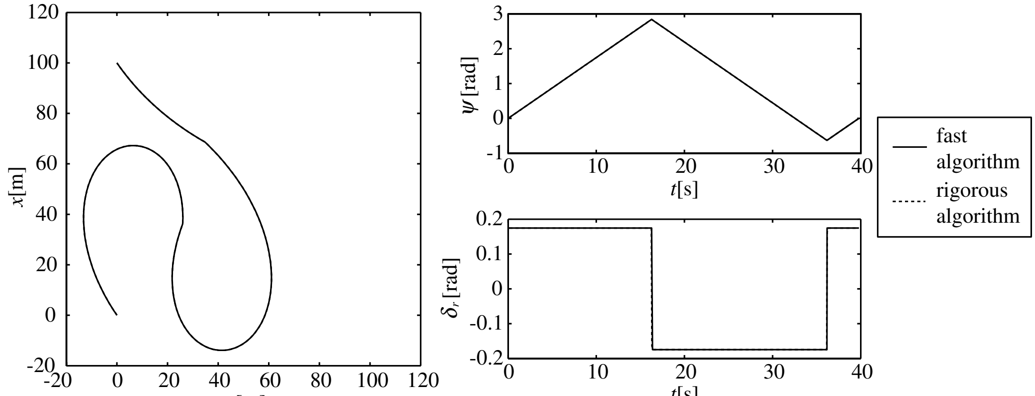

Fig. 7 Paths for case 1 calculated by the fast algorithm and the rigorous algorithm.

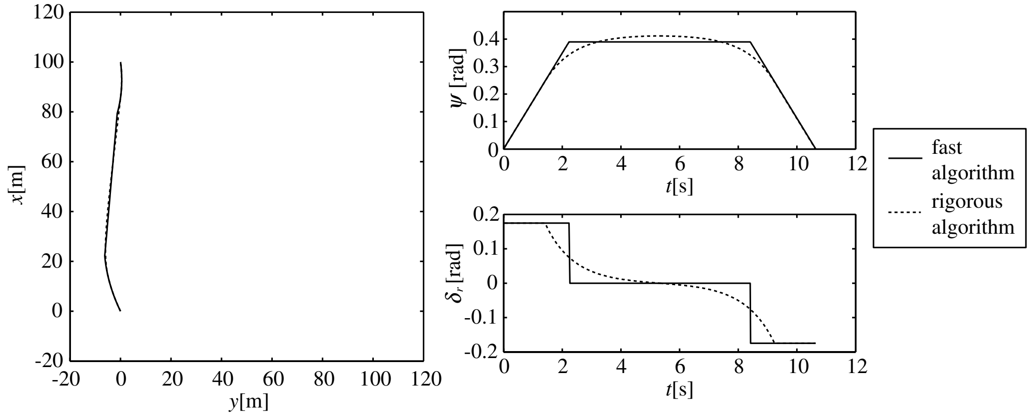

Fig. 8 Paths for case 2 calculated by the fast algorithm and the rigorous algorithm.

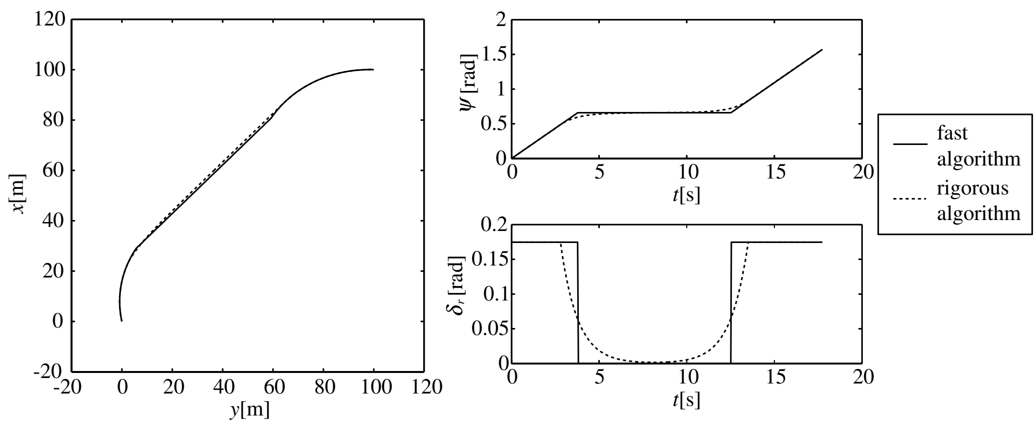

Fig. 9 Paths for case 3 calculated by the fast algorithm and the rigorous algorithm.

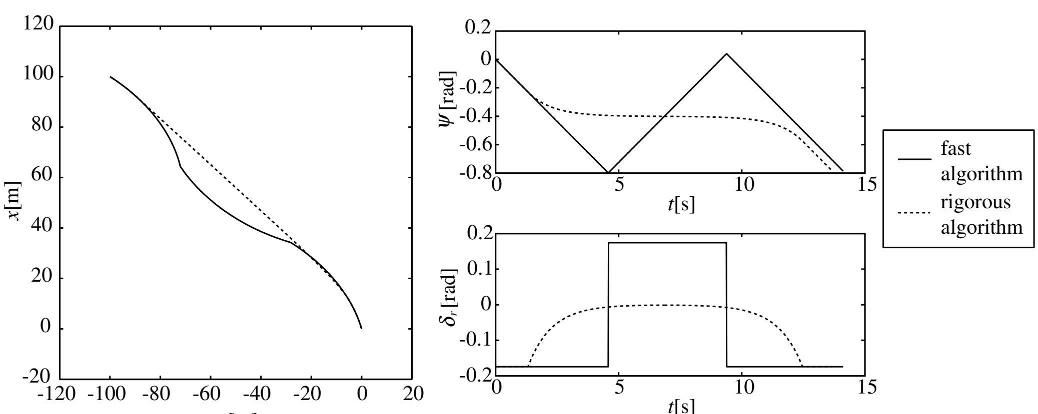

Fig. 10 Paths for case 4 calculated by the fast algorithm and the rigorous algorithm.

negligible. Thus, the paths of the fast algorithm in these cases exhibit sufficient quasi-optimality. On the other hand, in case 4, the path as calculated by the fast algorithm was clearly different from that of the rigorous algorithm, as shown in Fig. 10. Nevertheless, the increase in the total elapsed time of the path calculated by the fast algorithm was still admissible because it was approximately 3% of the total time of the optimal path.

By setting $a_\beta = 0$ in the fast algorithm, we also calculated the Dubins paths under the constant wind conditions. Figure 11 shows comparisons between the Dubins paths ($a_\beta = 0$) and paths calculated by the rigorous algorithm ($a_\beta \neq 0$). The differences of the paths are significant, and hence we can confirm the importance of using the skid-to-turn model ($a_\beta \neq 0$) as opposed to the simpler Dubins model ($a_\beta = 0$).

Next, we executed 10^6 random runs of the fast algorithm to check the computational speed and reliability of the convergence. In these random runs, the initial condition was fixed to $(x_0, y_0, \psi_0) = (0, 0, 0)$ without loss of generality. The terminal condition and the wind vector were given as follows:

$$x_f = 500 - 1000z_1, \qquad y_f = 500 - 1000z_2, \qquad \psi_f = 2\pi z_3$$
$$w_x = 9.5z_4 \cos(2\pi z_5), \qquad w_y = 9.5z_4 \sin(2\pi z_5) \tag{83}$$

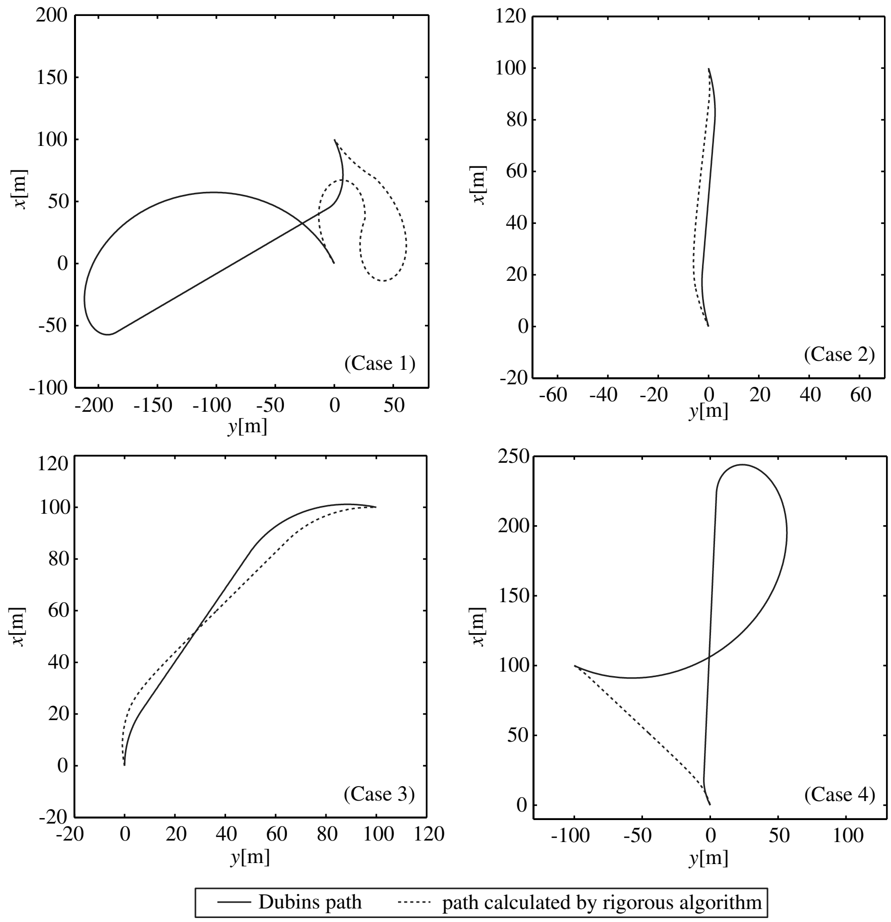

Fig. 11 Dubins paths ($a_\beta = 0$) and paths calculated by the rigorous algorithm ($a_\beta \neq 0$).

where $z_1, \ldots, z_5$ are independent uniform random numbers within the domain of $(0, 1)$. The fast algorithm successfully found the feasible paths in all of the 10^6 random runs. This demonstrates the guaranteed convergence of the fast algorithm. For all of the random runs, we used a desktop computer equipped with an Intel Core-2 Duo 2.4 GHz processor. Table 2 shows the statistics of the computational time. The maximum computational time was far less than 1 ms. On the other hand, the admissible time for onboard computation of the path planning would be more than 1 s when it is used for navigation of UAVs. Therefore, it would be possible to implement the fast algorithm even if a less capable onboard processor was installed in the vehicle and other computational processes required extra computational time.

Table 1 Total elapsed times of the paths calculated by the fast algorithm and the rigorous algorithm

Case no.	Fast algorithm	Rigorous algorithm	Difference
1	39.78 s	39.78 s	1.67×10^{-4} s
2	10.64 s	10.63 s	8.65×10^{-3} s
3	17.74 s	17.73 s	1.20×10^{-2} s
4	14.12 s	13.67 s	4.46×10^{-1} s

Table 2 Computational time of the fast algorithm

Mean	61.9 μs
Standard deviation	30.1 μs
Maximum	280 μs

Conclusions

In this study, two types of path planning algorithms were described for skid-to-turn UAVs, both of which calculate paths between two waypoints under constant wind conditions. One is a rigorous optimization algorithm based on the Euler–Lagrange formulation with analytical integration of the path. The other is a fast algorithm describing the path by two circular arcs connected by a line segment or another circular arc in the air mass frame, similar to the Dubins path. We compared the qualities of the paths calculated by the fast algorithm with those calculated by the rigorous optimization algorithm. In the sense of time minimization, the quasi-optimality of the paths calculated by the fast algorithm was observed. We also presented the convergence proof of the fast algorithm and confirmed its fast computational speed as well as the 100% convergence characteristics by running the fast algorithm in an extensive range of situations. These results indicate the potential and the effectiveness of the fast algorithm as an airborne path planner.

Proposed areas for future study include an investigation into the actual implementation of the fast algorithm on the onboard computer of a skid-to-turn UAV and the extension of the algorithm to paths in which the airspeed and altitude change.

Acknowledgments

The authors express their thanks to H. Adachi and T. Yamashita of NEC Corporation for motivating the authors to develop the algorithms.

References

[1] Wilson, J. R., "UAV Worldwide Roundup 2007," *Aerospace America*, Vol. 45, No. 5, May 2007, pp. 30–37.

[2] Thomasson, P. G., "Guidance of a Roll-Only Camera for Ground Observation in Wind," *Journal of Guidance, Control, and Dynamics*, Vol. 21, No. 1, 1998, pp. 39–44.
doi:10.2514/2.4230

[3] Rysdyk, R., "Unmanned Aerial Vehicle Path Following for Target Observation in Wind," *Journal of Guidance, Control, and Dynamics*, Vol. 29, No. 5, 2006, pp. 1092–1100.
doi:10.2514/1.19101

[4] Dubins, L., "On Curves of Minimal Length with a Constraint on Average Curvature, and with Prescribed Initial and Terminal Positions and Tangents," *American Journal of Mathematics*, Vol. 79, No. 3, 1957, pp. 497–516.
doi:10.2307/2372560

[5] Bui, X. N., Boissonnat, J. D., Soueres, P., and Laumond, J. P., "Shortest Path Synthesis for Dubins Non-Holonomic Robot," *Proceedings of 1994 IEEE International Conference on Robotics and Automation*, Inst. of Electrical and Electronics Engineers, Piscataway, NJ, 1994, pp. 2–7.

[6] Boissonnat, J. D., Cerezo, A., and Leblond, J., "Shortest Paths of Bounded Curvature in the Plane," *Journal of Intelligent and Robotic Systems: Theory and Applications*, Vol. 11, Nos. 1–2, 1994, pp. 5–20.
doi:10.1007/BF01258291

[7] Reeds, J. A., and Shepp, L. A., "Optimal Paths for a Car that Goes Both Forwards and Backwards," *Pacific Journal of Mathematics*, Vol. 145, No. 2, 1990, pp. 367–393.

[8] McGee, T. G., and Hedrick, J. K., "Optimal Path Planning with a Kinematic Airplane Model," *Journal of Guidance, Control, and Dynamics*, Vol. 30, No. 2, 2007, pp. 629–633.
doi:10.2514/1.25042

[9] McNeely, R. L., Iyer, R. V., and Chandler, P. R., "Tour Planning for an Unmanned Air Vehicle Under Wind Conditions," *Journal of Guidance, Control, and Dynamics*, Vol. 30, No. 5, 2007, pp. 1299–1306.
doi:10.2514/1.26055

[10] Tang, Z., and Ozguner, U., "Motion Planning for Multitarget Surveillance with Mobile Sensor Agents," *IEEE Transactions on Robotics*, Vol. 21, No. 5, 2005, pp. 898–908.
doi:10.1109/TRO.2005.847567

[11] Bicchi, A., Canaline, G., and Santiago, C., "Planning Shortest Bounded-Curvature Paths for a Class of Nonholonomic Vehicles Among Obstacles," *Journal of Intelligent and Robotic Systems: Theory and Applications*, Vol. 16, No. 4, 1996, pp. 387–405.
doi:10.1007/BF00270450

[12] Lee, J. I., and Ha, I. J., "Autopilot Design for Highly Maneuvering STT Missiles via Singular Perturbation-Like Technique," *IEEE Transactions on Control Systems Technology*, Vol. 7, No. 5, 1999, pp. 527–541.
doi:10.1109/87.784417

[13] Sreenatha, A. G., Rajhans, V., and Bhardwaj, N., "Robust Controller Design for a Skid to Turn Missile," *Acta Astronautica*, Vol. 45, No. 2, 1999, pp. 85–92.
doi:10.1016/S0094-5765(99)00107-1

[14] Chwa, D. K., and Choi, J. Y., "New Parametric Affine Modeling and Control for Skid-to-Turn Missiles," *IEEE Transactions on Control Systems Technology*, Vol. 9, No. 2, 2001, pp. 335–347.
doi:10.1109/87.911385.

[15] Beard, R. W., Curtis, J. W., Eilders, M., Evers, J., and Cloutier, J. R., "Vision Aided Proportional Navigation for Micro Air Vehicles," AIAA Paper 2007-6609, 2007.

[16] Etkin, B., *Dynamics of Atmospheric Flight*, Wiley, New York, 1972, Chaps. 4, 5.

[17] Bryson, A. E., Jr., and Ho, Y. C., *Applied Optimal Control*, Hemisphere, New York, 1975.

[18] Pontryagin, L. S., Boltyanskii, V. R., Gamkrelidze, R. V., and Mishchenko, E. F., *The Mathematical Theory of Optimal Processes*, Interscience, New York, 1962.

[19] Betts, J. T., "Survey of Numerical Methods for Trajectory Optimization," *Journal of Guidance, Control, and Dynamics*, Vol. 21, No. 2, 1998, pp. 193–207.
doi:10.2514/2.4231

[20] Betts, J. T., and Huffman, W. P., "Path-Constrained Trajectory Optimization Using Sparse Sequential Quadratic Programming,", *Journal of Guidance, Control, and Dynamics*, Vol. 16, No. 1, 1993, pp. 59–68.
doi:10.2514/3.11428

[21] Yokoyama, N., Suzuki, S., and Tsuchiya, T., "Convergence Acceleration of Direct Trajectory Optimization Using Novel Hessian Calculation Methods," *Journal of Optimization Theory and Applications*, Vol. 136, No. 3, 2008, pp. 297–319.
doi:10.1007/s10957-008-9351-0

[22] Ohtsuka, T., "A Continuation/GMRES Method for Fast Computation of Nonlinear Receding Horizon Control," *Automatica*, Vol. 40, No. 4, 2004, pp. 563–574.
doi:10.1016/j.automatica.2003.11.005

[23] Brent, R. P., *Algorithms for Minimization without Derivatives*, Prentice–Hall, Upper Saddle River, NJ, 1973, Chaps. 3, 4.